# Classical collisional trajectories as the source of strong-field double ionization of helium in the knee regime

Li-Bin Fu,[1] Jie Liu,[1,2] Jing Chen,[2,3] and Shi-Gang Chen[1]
[1]*Institute of Applied Physics and Computational Mathematics, P. O. Box 8009 (26), 100088 Beijing, China*
[2]*CCAST (World Laboratory), P. O. Box 8730, Beijing, China*
[3]*Institute of Theoretical Physics, Chinese Academy of Science, P. O. Box 2735, Beijing 100080, China*
(Received 16 November 2000; published 20 March 2001)

In this paper, the quasistatic model is extended to describe the double ionization of helium in an intense linearly polarized field, yielding insight into the two-electron correlation effect in the ionization dynamics. Our numerical calculations reproduce the excessive double ionization and the photoelectron spectra observed experimentally both quantitatively and qualitatively. Moreover, it is shown that the classical collisional trajectories are the main source of the double ionization in the knee regime where the double ionization yield is much higher than that predicted by the sequential single active electron models, and responsible for the unusual angular distribution of the photoelectrons.

DOI: 10.1103/PhysRevA.63.043416 PACS number(s): 32.80.Rm, 42.50.Hz, 31.15.−p

Recently, the excessive double ionization observed in helium experiments by Fittinghoff *et al.* [1], Walker *et al.* [2], and Sheehy *et al.* [3] has drawn much attention to multiple-electron dynamics in laser-atom interactions. In these experiments the single ionization yield of He in a linearly polarized field is accurately predicted by the single active electron (SAE) approximation [2], well described by the Ammosov-Delone-Krainov (ADK) tunneling theory [4]. However, the case of double ionization is more complicated. In the regime of very high intensities ($I>10^{16}$ W/cm$^2$), where strong double ionization occurs, the double ionization is in good agreement with the sequential SAE models as is that in the lower intensity regime ($I<10^{14}$ W/cm$^2$). The double ionization yield deviates seriously from the sequential SAE model and shows great enhancement in the knee regime [$(0.8–3.0)\times10^{15}$ W/cm$^2$], where the $He^{2+}/He^{+}$ yield ratio is close to a constant: 0.002. This surprisingly large yield of double ionization obviously indicates that sequential ionization is no longer the dominating process in this regime and that electron-electron correlation has to be taken into account.

Both the shake-off model and the recollision model have been suggested to describe the electron correlation [1,3,5,6]. However, neither of these two nonsequential ionization (NSI) mechanisms can completely explain the experimental observations. The shake-off model cannot explain the decrease in the double ionization yields as the polarization of the laser field departs from linear [7–9]. In the recollision model, the returning electrons are known to have a maximum classical kinetic energy of $\sim 3.2U_p$ ($U_p = e^2F^2/4m_e\omega^2$), so one can determine the minimum intensity required for the rescattering electron to have enough energy to excite the inner electron. But the double ionization yields observed in experiments have no such intensity threshold. In fact, the double ionization process is rather complicated and subtle; both the two NSI processes and sequential ionization contribute to the double ionization yields and may dominate in the different regimes. In another approach, Becker and Faisal proposed a ''correlated energy sharing'' model to describe the NSI processes and nuclei recoil experimental [10–12]. The model is based on the so-called intense-field many-body *S*-matrix theory derived by a rearrangement of the usual *S*-matrix series and includes time, electron correlation, and the rescattering mehanism.

The experiments on the double ionization of helium are mainly confined to the tunneling regime, i.e., the ratio between the tunneling time of the outer electron and the inverse optical frequency (Keldysh parameter) is less than 1. In this regime, the quasistatic model [5] provides a perfect description for hydrogenlike atoms in intense fields and successfully explains most nonlinear phenomena observed experimentally [5,13,14]. Inspired by this success, in this paper we extend it to develop a three-dimensional 3D quasistatic model (a two-step process) which we use to investigate the mechanism of double ionization of helium by tracing the classical trajectories of the two correlated electrons. We attribute the double ionization to the classical collisional trajectories: Distinct trajectory configurations corresponding to the shake-off and recollision mechanisms contribute to the nonsequential double ionization of helium. Our numerical simulations successfully reproduce the excessive double ionization and the photoelectron spectra observed experimentally in the knee regime. An intuitive picture of double ionization will be provided by this model.

As a beginning, we present the improved two-step quasistatic model adopted in our calculations. The first step, where the outer electron tunnels free, is treated by the tunneling ionization theory generalized by Delone and Krainov [15]. In the second step, the evolution of the two electrons after the first electron has tunneled and the electron-electron interaction are described by the classical equations (in atomic units)

$$\frac{d^2\mathbf{r}_1}{dt^2} = -\frac{2\mathbf{r}_1}{r_1^3} + \frac{\mathbf{r}_1-\mathbf{r}_2}{|\mathbf{r}_1-\mathbf{r}_2|^3} - \mathbf{F}(t), \tag{1}$$

$$\frac{d^2\mathbf{r}_2}{dt^2} = -\frac{2\mathbf{r}_2}{r_2^3} - \frac{\mathbf{r}_1-\mathbf{r}_2}{|\mathbf{r}_1-\mathbf{r}_2|^3} - \mathbf{F}(t), \tag{2}$$

where $\mathbf{F}(t)$ is the laser field.

 

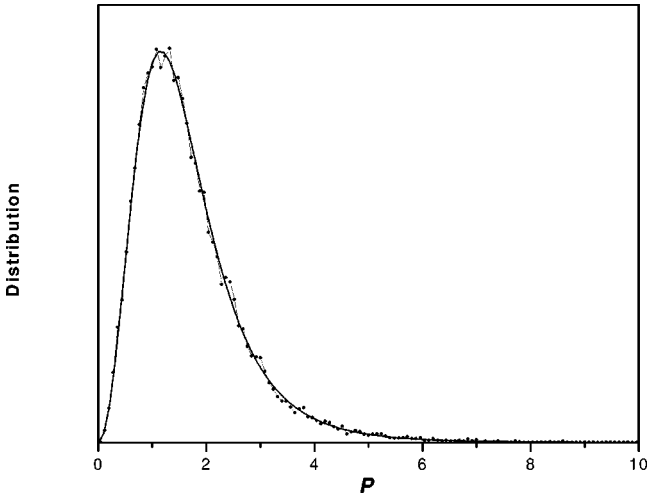


FIG. 1. Momentum distribution of the initial state of the inner electron. The full circles denote the results of $10^4$ Monte Carlo points; the solid line is the distribution given by the formula (4).

In our model, the initial state of the inner electron of helium is described by a microcanonical distribution that is widely used in the classical-trajectory Monte Carlo (CTMC) method established and developed in [16,17]. The CTMC method has been successfully used in studying the interaction of atoms with strong laser fields by numerous authors [18,19]. It provides a statistical distribution of all the parameters defining the initial conditions of the trajectory of electrons in the ground state of a hydrogenlike atom. Thus, the initial distribution of the inner electron is

$$\rho(\mathbf{r}_2,\mathbf{p}_2)=\frac{\delta(E_2-H_0(r_2,p_2))}{K}, \tag{3}$$

where $H_0(r_2,p_2)=p_2^2/2m_e-Ze^2/r_2$, $K$ is the normalization constant, and $E_2=-2$ a.u. is the eigenenergy of the inner electron. Integrating the above equation, one obtains the momentum distribution

$$\rho(\mathbf{p}_2)=\frac{8p_c^5}{\pi^2(p_2^2+p_c^2)^4}, \tag{4}$$

in which $p_c^2=2m_eU$ and $U$ is the negative energy of the inner electron.

The spherically symmetric ground-state $He^+$ is represented by the above microcanonical distribution. This state is specified by the binding energy of the electron in the target atom and five additional parameters randomly distributed in the following ranges: $-\pi\leqslant\phi\leqslant\pi$, $-1\leqslant\cos\theta\leqslant1$, $-\pi\leqslant\eta<\pi$, $0\leqslant\epsilon^2\leqslant1$, and $0\leqslant\chi_n\leqslant2\pi$ [17]. Here, $\epsilon$ is the eccentricity of the orbit, $\chi_n$ is a parameter of the orbit proportional to time, and $\phi$, $\theta$, and $\eta$ are Euler angles. A random distribution of these parameters corresponds to equal probability of the inner electron having any phase in its periodic motion. Here, $10^4$ initial points are chosen and their momentum distribution is compared with Eq. (4). Figure 1 shows that they are in agreement.

The initial condition of the tunneled electron, under the SAE approximation for $He^+$, is determined by an equation including the effective potential given in Ref. [20] and a generalized tunneling formula developed by Delone and Krainov [15]. In parabolic coordinates, the Schrödinger equation for a hydrogenlike atom in a uniform field $\epsilon$ is written (in atomic units)

$$\frac{d^2\phi}{d\eta^2}+\left(\frac{I_{p1}}{2}+\frac{1}{2\eta}+\frac{1}{4\eta^2}+\frac{1}{4}\epsilon\eta\right)\phi=0, \tag{5}$$

in which $I_{p1}=-0.9$ a.u. is the negative ionization potential of the outer electron.

The above equation has the form of a one-dimensional Schrödinger equation with the potential $U(\eta)=-1/4\eta-1/8\eta^2-\epsilon\eta/8$ and the energy $K=I_{p1}/4$. The turning point for an electron tunneling at time $t_0$ is determined by $U(\eta)=K$. In the quasistatic approximation, the field parameter $\epsilon$ is related to the laser field amplitude $F(t)$ by $\epsilon=F(t_0)$. One must point out that, when $\epsilon>F_{th}$, the turning point will be complex, which determines the threshold value of the field $F_{th}=0.338$ a.u.

The evolution of the outer electron is traced by launching a set of trajectories with different initial parameters $t_0$ and $v_{1x0}$, where $v_{1x0}$ is the initial velocity perpendicular to the polarization of the electric field. The initial position of the electron tunneling at time $t_0$ is given by $x_{10}=y_{10}=0, z_{10}=-\eta_0/2$ from Eq. (5). The initial velocity is set to be $v_{1y0}=v_{1z0}=0, v_{1x0}=v_{10}$. Thus, the weight of each trajectory is evaluated by [15]

$$w(t_0,v_{10})=w(0)w(1), \tag{6}$$

$$w(1)=\frac{\sqrt{2I_{p1}}v_{10}}{\epsilon\pi}\exp(-\sqrt{2I_{p1}}v_{10}^2/\epsilon), \tag{7}$$

where $w(0)$ is the tunneling rate in the quasistatic approximation [21].

Before we go further, we would like to compare our model with a similar model [22] describing the double ionization of helium. First, in our model the initial condition of the inner electron is given by the classical-trajectory Monte Carlo method; second, the Coulomb interaction is described by the real Coulomb potential. These improvements are essential. In the model given in Ref. [22], the inner electron is assumed to be at rest at the center. This initial condition confines the motion of both electrons in the same plane defined by the polarization axis and the direction of the initial transverse momentum, i.e., in fact, the calculations in that paper are for a 2D system, which may increase the probability of collisions between the two electrons. On the other hand, the softened Coulomb potential approximation adopted in Ref. [22] makes the inner electrons more easily excited and causes an overestimation of the double ionization rate. Our model has been employed to understand the momentum distribution of the recoil ions and shows good agreement with the experimental records [23]. Here, we note that there are several works in which the classical-trajectory treatment was used to describe above-threshold ionization [24,25].

In our calculation, Eqs. (1) and (2) are solved in a time interval between $t_0$ and $13T$ by employing the standard Runge-Kutta algorithm. After ten optical cycles the electric field is switched off using a $\cos^2$ envelope during three cycles, and during the last two optical cycles the electrons is free from the electric field. So the electric field can be expressed as

$$\mathbf{F}(t) = a(t) F \cos(\omega t)\mathbf{e}_z, \tag{8}$$

where $F$ and $\omega$ are the amplitude and frequency of the field, respectively, and the envelope function $a(t)$ is defined by

$$a(t) = \begin{cases} 1, & t \leqslant 10T \\ \cos^2 \dfrac{(t-10T)\pi}{6T}, & 10 < t \leqslant 13T \\ 0, & t > 13T. \end{cases} \tag{9}$$

The wavelength is $\lambda = 780$ nm, which is chosen to match the experiment [2], and the intensities range from $I = 10^{14}$ W/cm$^2$ to the threshold value $I = 4 \times 10^{15}$ W/cm$^2$.

In our computations, $10^5$ or more initial points are randomly distributed in the parameter plane $-\pi/2 < \omega t_0 < \pi/2, v_{1x0} > 0$ for the outer electron and in the microcanonical distribution for the inner electron. The probability for double ionization and the angular distribution can be obtained by statistical analysis of an ensemble of classical trajectories weighted according to Eq. (6). The results have been tested for numerical convergence by increasing the number of trajectories.

In our treatment, the behavior of the classical trajectories plays an important role and determines the ionization dynamics of the electrons. There are four kinds of typical trajectory. Figure 2(a) shows a simple behavior. After tunneling out, the outer electron is driven mainly by the field and directly moves away. It collides neither with the core nor with the inner electron. Figure 2(b) gives a more complicated picture in which multiple returns and long-time trapping are experienced by the outer electron. The outer electron first tunnels out, and then oscillates in the combined laser and Coulomb fields. After several optical periods, it collides with the core and then absorbs enough energy to escape. In these two cases, no double ionization occurs since collisions between the two electrons are not probable or slight. Figures 2(c) and 2(d) give typical pictures of the double ionization process. In Fig. 2(c), the outer electron tunnels at the moment close to the peak of the electric field and oscillates in the combined laser and Coulomb fields. After several optical periods, it returns to the neighborhood of the core and collides strongly with the inner electron. This collision provides enough energy for the inner bounded electron to get free. Figure 2(d) shows that, after the outer electron has tunneled, the laser field reverses its direction within less than a quarter of the optical period, so that this electron is driven back, collides with the inner electron near the core, and ionizes it. As we will show later, the resulting energy spectra and the angular distributions of the photoelectrons for the two processes are quite distinct.

To match the experiments, Fig. 3 shows the double ionization yields of helium calculated by our model at 13 different intensities in the range $(4 \times 10^{14})$–$(4 \times 10^{15})$ W/cm$^2$. The dashed line is the single ionization yield of He predicted by the ADK tunneling rate [4], and the dotted line is the ADK tunneling rate for $He^+$. For peak intensities below $3 \times 10^{15}$ W/cm$^2$, one sees that the double ionization rate obtained from our numerical simulations is larger than the ADK tunneling rate, but for intensities above $3 \times 10^{15}$ W/cm$^2$ the ADK tunneling rate increases rapidly and becomes larger than the ionization rate given by our model. This figure shows that our calculation is able to reproduce, qualitatively at least, the excessive double ionization observed in helium experiments [2]. The inset in Fig. 3 shows the double ionization rate calculated by our model normalized to the ADK tunneling rate of He versus the intensity. Our result is in good agreement with the data in the knee regime observed in experiments [2]: the $He^{2+}/He^+$ ratio in the knee regime is around 0.002. At lower intensities ($I < 0.5 \times 10^{15}$ W/cm$^2$), the deviation between our calculation and the experimental records becomes serious. In a word, our model provides a suitable description for the double ionization in the knee regime, where as shown above the classical collisional trajectories [Figs. 2(c) and 2(d)] are believed to be the main source of the double ionization. Above this regime, tunneling ionization of the inner electron becomes possible and the ADK description is available. Below this regime, the ionization mechanism of the outer electron transits from the tunneling regime to the multiphoton regime and the tunneling description is no longer appropriate.

Figure 4 shows the relations between the ionization rate and the phase of the laser field when the outer electron tunneled. One finds that the double ionization yields mainly come from the region $-0.2 < \omega t_0 < 0.4$ close to the peak of the electric field. There is a tail in the regime $\omega t_0 > 0.4$ and a cutoff for $\omega t_0 < -0.2$. We know that when the outer electron tunnels out near the peak of the laser field its canonical momentum is almost zero. Hence, the outer electron tends to oscillate in the combined laser and Coulomb fields for several optical periods, and then returns to the neighborhood of the core to collide with the inner electron. In this case, the typical trajectory of the double ionization process corresponds to Fig. 2(c). For phase $\omega t_0 < -0.2$, the tunneled electrons have a nonzero canonical momentum directed outward from the core. Consequently, they will be driven by the laser field and escape directly from the core. That is, in this process, the outer electron has no chance to return to the core and no double ionization occurs. For phase $\omega t_0 > 0.4$, the outer tunneled electron has a nonzero canonical momentum toward the core, and soon after it has tunneled out the laser field also reverses its own direction to the same direction. So the electron is driven back to the core by the external field and collides with the inner electron. Figure 2(d) shows the typical trajectory for this case. In this region the tunneling ionization of the outer electron is not efficient, and the double ionization rate is low. Comparing the two typical processes of double ionization, one can find some intrinsic differences. In Fig. 2(c) the outer electron was first ionized out and then driven by the field to collide with the inner electron

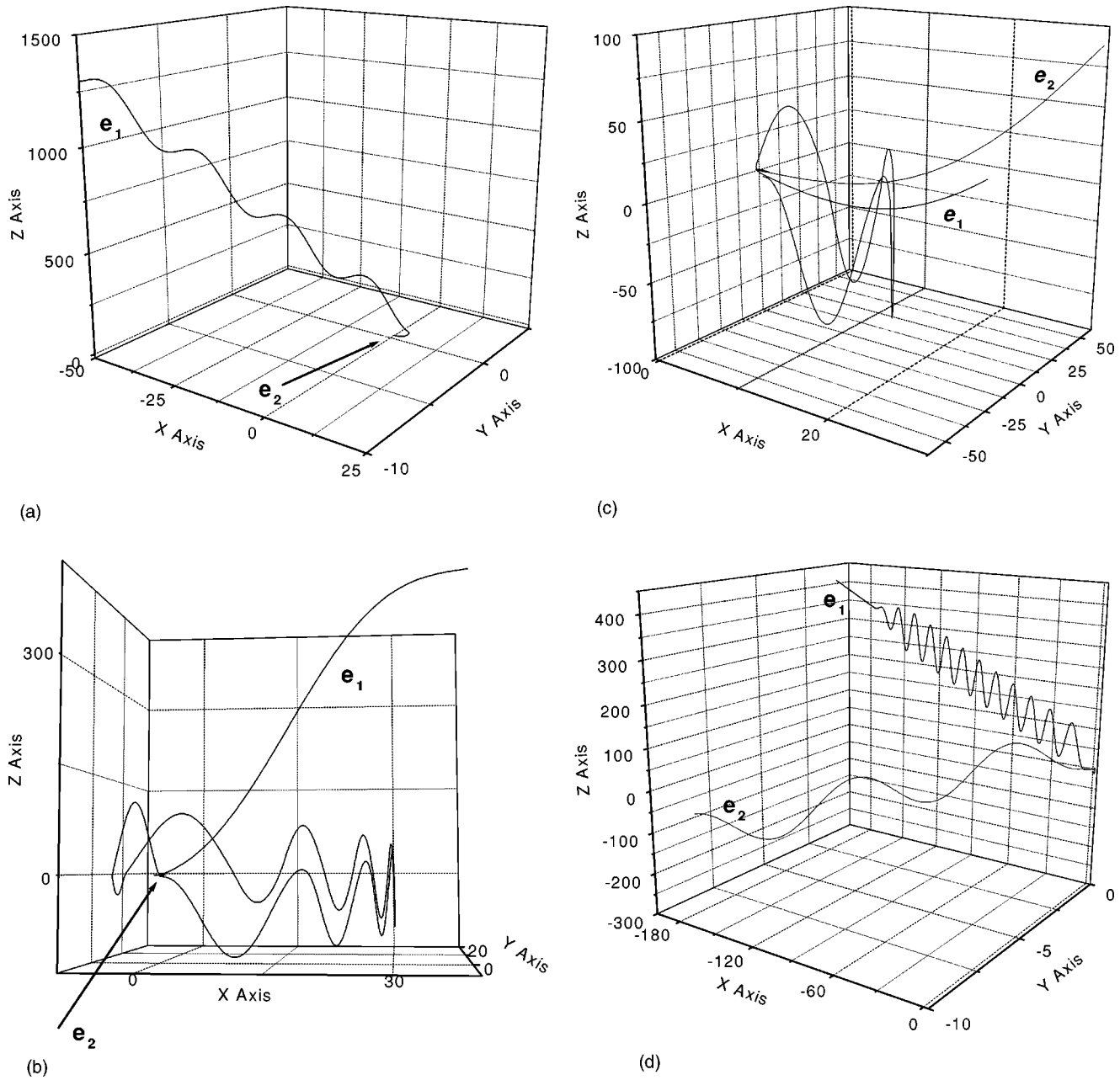


FIG. 2. Four typical trajectories. (a) The final energies are $E_1=4.694$ a.u. and $E_2=-2.01$ a.u., and the emission angle of the outer electron $\theta=2.26°$; (b) The final energies are $E_1=8.683$ a.u. and $E_2=-1.153$ a.u., and the emission angle of the outer electron $\theta=5.67°$. (c) The typical trajectories of electrons in double ionization correspond to $\omega t_0$ in the phase interval $(-0.2,0.4)$. The initial $\omega t_0=-0.087$, the weight of the trajectory is 0.168, the final energies are $E_1=3.407$ a.u., $E_2=3.278$ a.u., and the emission angles of the two electrons are $\theta_1=25.15°, \theta_2=30.86°$. (d) The typical trajectories of electrons in double ionization correspond to the phase interval $(\omega t_0>0.4)$. Here $\omega t_0=0.924$, the weight of the trajectory is 0.014, the final energies are $E_1=2.663$ a.u., $E_2=0.237$ a.u., and the emission angles of the two electrons $\theta_1=19.2°, \theta_2=129.0°$.

and cause the double ionization, which is a typical picture of the recollision process. In Fig. 2(d) the inner electron was ionized during the process when the outer electron was driven away from core by the external field; both electrons ionize simultaneously, which possesses the properties of the shake-off mechanism. The difference between the two processes, manifested clearly in the energy evolution of the two electrons. As shown in Fig. 5(a), the outer electron becomes free with a positive energy and then comes back to collide with the inner electron. This collision causes a sudden increment in the energy of the inner electron, which soon becomes free. Because the collision between the two electrons is almost instantaneous the energy is approximately conserved when the collision happens. In the case of Fig. 5(b), during the escape process of the outer electron it collides with the inner one. Consequently, both electrons become free almost simultaneously. From our calculation we know that both processes contribute to the double ionization in the knee

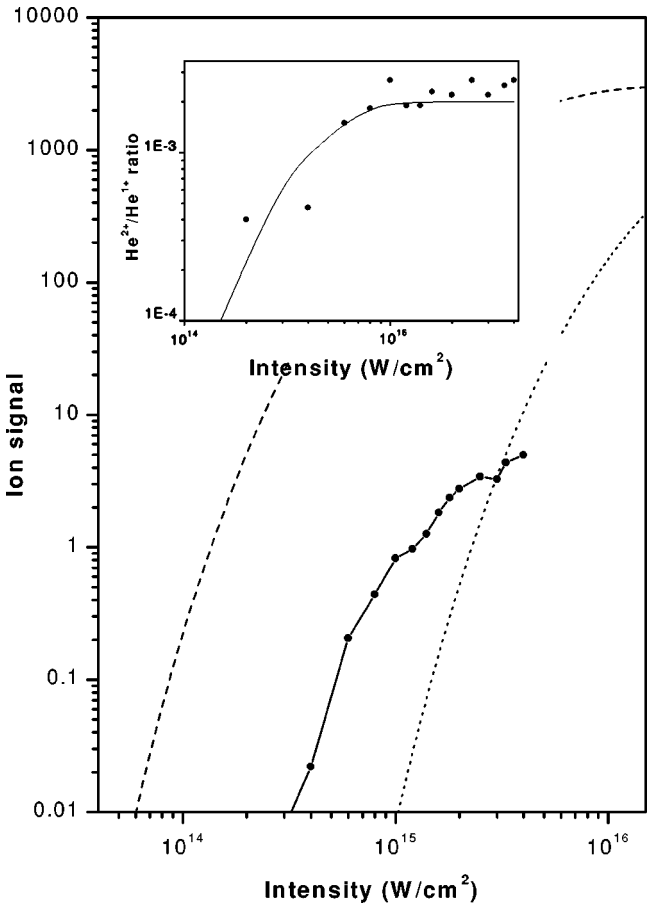


FIG. 3. The dashed and dotted lines correspond to the single ionization yields of He and $He^+$ predicted by ADK tunneling ionization; the full circles correspond to the results from our model. Inset: Intensity dependence of $He^{2+}/He^+$ ratio given by our model. The solid line is from the experiment [2].

region, but the main contribution comes from the recollision process, which gives more than 80% of the double ionization yield.

From our calculations, we can also obtain the photoelectron spectra (PES) and the photoelectron angular distribution

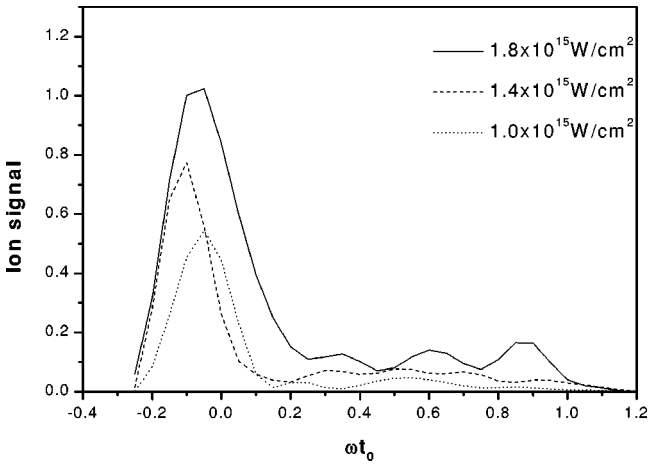


FIG. 4. The double ionization of He versus the phase of the laser field at the moment when the outer electron tunneled.

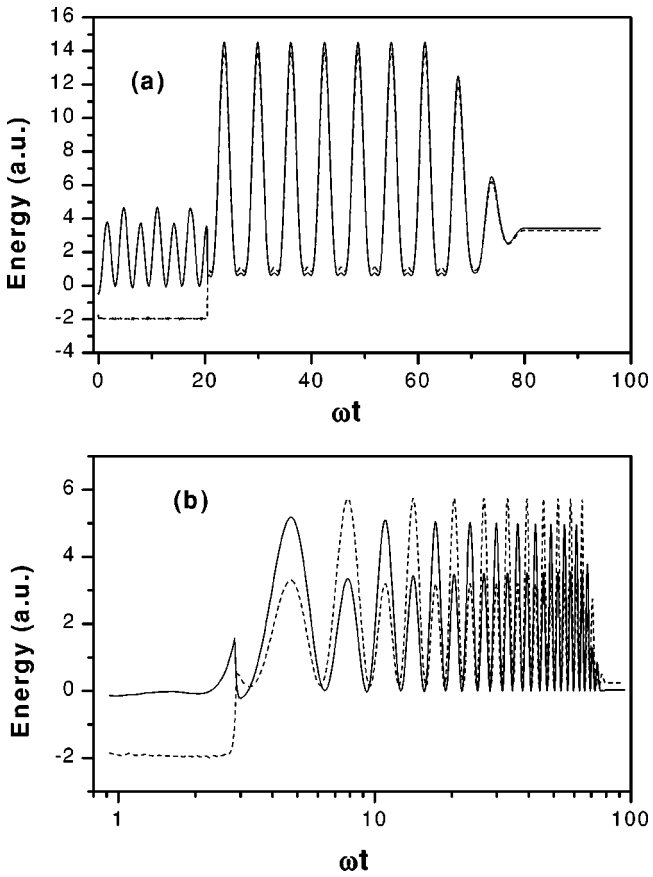


FIG. 5. The energy evolution of the two electrons during the double ionization process (a) corresponding to the case of Fig. 2(c), and (b) corresponding to the case of Fig. 2(d). The solid line represents the outer electron and the dashed line represents the inner electron.

(PAD). Figure 6 shows the total photoelectron energy distribution at $1\times10^{15}$ W/cm$^2$ and at $1.6\times10^{15}$ W/cm$^2$ (both in the knee regime) calculated from our model. One can see that, in absolute units, an increasing laser intensity results in an increase of higher energy photoelectrons. But if one scales the energy units by the pondermotive energy $U_p = e^2F^2/4m_e\omega^2$ of the electron, one finds that the PES for

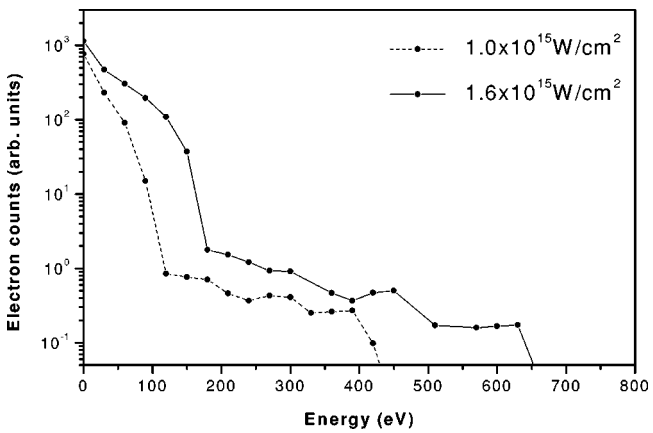


FIG. 6. Photoelectron energy spectra calculated from our model.

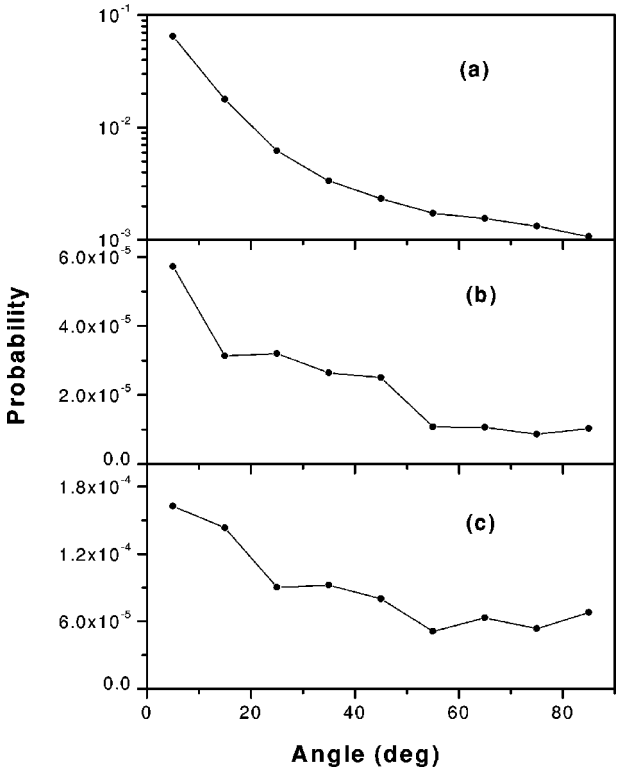


FIG. 7. Photoelectron angular distribution at $2\times10^{15}$ W/cm$^2$. (a) shows the total distribution of photoelectrons; (b) PAD for photoelectrons in energy region II; (c) PAD of the photoelectrons in double ionization.

both intensities shows a similar shape: The spectrum exhibits a sharply decreasing slope (region I, $0-2U_p$) followed by an extended plateau up to $8U_p$ or more (region II). This spectral structure is much closer to experimental observations in this regime [2].

We know that in our model the electron tunneling is initiated in the phase interval $[-\pi/2,\pi/2]$, so the total photoelectron angular distribution has to consider the contribution of electrons originating in $[\pi/2,3\pi/2]$, which is rotated by 90°. Figure 7(a) is the total angular distribution of ionized electrons. One finds that, except for a concentration in the field direction, there exists a long tail decreasing with a power-law dependence $1/\sin^r(\theta/2)$, which is different from the angular distribution for pure tunneling where it decreases exponentially. This structure is due to the scattering from the core and the interaction between two electrons during the rescattering process. Figure 7(b) shows the angular distribution of photoelectrons in the energy region II. The most striking feature of the plot is the existence of a slight slope up to 40° followed by a tail up to 90°. If one compares this result with the angular distribution of the transition region in rescattering processes described in Ref. [13], where there are no photoelectrons emitted at angles much larger than 40°, it is not difficult to conclude that the tail structure is due to the electron-electron interactions. Because the velocity direction of the inner electron is random when the collision happens, the instantaneous strong interactions can give rise to large emission angles of the photoelectron. This can be verified from Fig. 7(c), which shows the total angular distribution of photoelectrons in double ionization. The angular distribution is almost flat and decreases slowly as the emission angle increases.

In fact, the final energy and angular distribution of the photoelectrons are mainly determined by the scattering processes. The process shown in Fig. 2(a) produces only a low energy photoelectron (region I) with small emission angle. However, for the process shown in Fig. 2(b), the classical trajectories have complex behavior, and the energy exchange in this process is also complicated. The multiple returns and long-time trapping can produce high energy electrons in this process. So this process contributes to the high energy part of the PES. It is also found that the structures of the PES and PAD are similar to some extent to those from the rescattering model of hydrogen [13]. This fact indicates that the main structures of PES and PAD come from the rescattering process of the outer electron with the ion $He^+$.

In conclusion, a quasistatic two-step model was used to investigate the double ionization of helium in an intense linearly polarized field. Our calculations reproduce the excessive double ionization and the photoelectron spectra observed in experiments. We argue that the classical collisional trajectories are the main source of the double ionization in the knee regime and responsible for the unusual angular distribution of the photoelectrons. Two distinct typical collisional trajectories correspond to the recollision process and the shake-off process, respectively. Both processes contribute to the double ionization, but the recollision gives the main contribution and leads to more than 80% of the double ionization yields. Our calculations based on classical trajectories provide an intuitive picture of the double ionization of helium, and are helpful in understanding the complicated behavior of multielectron atoms in intense laser fields obtained in quantum calculations and future experiments.

We acknowledge very helpful discussions with Dr. T. W. Cheng. This work was supported by the Important Fundamental Research Project of China.

[1] D.N. Fittinghoff, P.R. Bolton, B. Chang, and K.C. Kulander, Phys. Rev. Lett. **69**, 2642 (1992).
[2] B. Walker, B. Sheehy, L.F. DiMauro, P. Agostini, K.J. Schafer, and K.C. Kulander, Phys. Rev. Lett. **73**, 1227 (1994).
[3] B. Sheehy, R. Lafon, M. Widmer, B. Walker, L.F. DiMauro, P.A. Agostini, and K.C. Kulander, Phys. Rev. A **58**, 3942 (1998).
[4] M.V. Ammosov, N.B. Delone, and V.P. Krainov, Zh. Éksp. Teor. Fiz. **91**, 2008 (1986) [Sov. Phys. JETP **64**, 1191 (1986)].
[5] P.B. Corkum, Phys. Rev. Lett. **71**, 1994 (1993).
[6] K.C. Kulander, J. Cooper, and K.J. Schafer, Phys. Rev. A **51**, 561 (1995).

[7] B. Walker, E. Mevel, B. Yang, P. Breger, J.P. Chambaret, A. Antonetti, L.F. DiMauro, and P.A. Agostini, Phys. Rev. A **48**, R894 (1993).
[8] D.N. Fittinghoff, P.R. Bolton, B. Chang, and K.C. Kulander, Phys. Rev. A **49**, 2174 (1994).
[9] K. Kondo, A. Sagisaka, T. Tamida, Y. Nabekawa, and S. Watanabe, Phys. Rev. A **48**, R2531 (1993).
[10] A. Becker and F.H.M. Faisal, J. Phys. B **32**, L335 (1996).
[11] A. Becker and F.H.M. Faisal, Phys. Rev. A **59**, R1742 (1999).
[12] A. Becker and F.H.M. Faisal, Phys. Rev. Lett. **84**, 3546 (2000).
[13] B. Hu, J. Liu, and S.G. Chen, Phys. Lett. A **236**, 533 (1997).
[14] J. Chen, J. Liu, and S.G. Chen, Phys. Rev. A **61**, 033402 (2000).
[15] N.B. Delone, and V.P. Krainov, J. Opt. Soc. Am. B **8**, 1207 (1991).
[16] R. Abrines and I.C. Percival, Proc. Phys. Soc. London **88**, 861 (1966); J.G. Leopold and I.C. Percival, J. Phys. B **12**, 709 (1979).
[17] J.S. Cohen, Phys. Rev. A **26**, 3008 (1982).
[18] C.H. Keitel and P.L. Knight, Phys. Rev. A **51**, 1420 (1995); G. Bandarage *et al.*, *ibid.* **46**, 380 (1992); M. Gajda *et al.*, *ibid.* **46**, 1638 (1992); G.A. Kyrala, J. Opt. Soc. Am. B **4**, 731 (1992).
[19] J. Liu, S.G. Chen, and D.H. Bao, Commun. Theor. Phys. **25**, 129 (1996).
[20] L.D. Landau and E. M. Lifishitz, *Quantum Mechanics* (Pergamon, Oxford, 1977).
[21] A.M. Perelomov, V.S. Popov, and V.M. Teren'ev, Zh. Éksp. Teor. Fiz. **50**, 1393 (1966) [Sov. Phys. JETP **23**, 924 (1966)]; M.V. Ammosov, N.B. Delone, and V.P. Krainov, *ibid.* **91**, 2008 (1986).
[22] T. Brabec, M.Yu. Ivanov, and P.B. Corkum, Phys. Rev. A **54**, R2551 (1996).
[23] J. Chen, J. Liu, L.B. Fu, and W.M. Zheng, Phys. Rev. A **63**, 011404(R) (2001).
[24] R. Kopold, W. Becker, and M. Kleber, Opt. Commun. **179**, 39 (2000).
[25] S.P. Goreslavsky and S.V. Popruzhenko, Phys. Lett. A **249**, 477 (1998).